THE JOURNAL OF PHYSICAL CHEMISTRY C

pubs.acs.org/JPCC Article

Hexagonal Boron Nitride Encapsulation of Organic Microcrystals and Energy-Transfer Dynamics

Published as part of The Journal of Physical Chemistry virtual special issue "Josef Michl Festschrift".

Wangxiang Li, Hao Tian, Jeremiah van Baren, Adam Berges, Mashael M. Altaiary, Erfu Liu, Elena Bekyarova, Chun Hung Lui, Jianlin Liu, and Christopher J. Bardeen*

Cite This: *J. Phys. Chem. C* 2020, 124, 21170–21177 Read Online

ACCESS | Metrics & More | Article Recommendations | Supporting Information

ABSTRACT: Ultrathin layers of hexagonal boron nitride (h-BN) are used to fully encapsulate single perylene microcrystals. The morphology and chemical stability for samples prepared using different encapsulation methods are characterized using electron, optical, and atomic force microscopies. Only multilayer MBE-grown h-BN could fully protect the organic crystals from dissolution and sublimation. To determine the interaction of the two-dimensional material with the underlying organic chromophores, a polymer film with Lumogen Red dye molecules that act as energy donors was used to characterize the fluorescence quenching ability of the encapsulation layer. Encapsulation using wet-transfer method leads to h-BN layers that have an effective Forster quenching radius of 2.9 nm, as compared to 14.6 nm for graphene. Fluorescence quenching by h-BN can be completely avoided by using dry-transfer methods, suggesting that wet transfer leads to structural defects that act as energy acceptors. Both the type of h-BN and its method of transfer determine its ability to act as an inert coating and avoid fluorescence quenching. Encapsulation of organic molecular crystals using multilayer h-BN is feasible, but attention must be paid to preparation conditions and the nature of the h-BN sample.

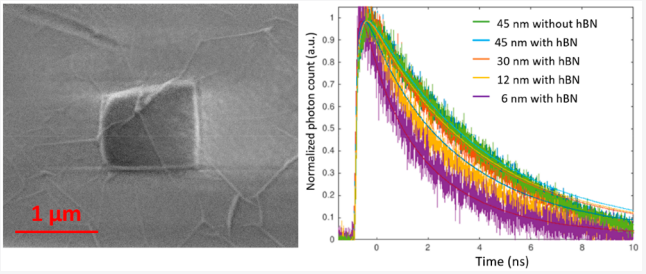

INTRODUCTION

Two-dimensional (2D) materials such as graphene are an area of intense research interest due to their unique electronic, mechanical, and optical properties.[1,2] In addition to their intrinsic properties, 2D materials can be combined with other materials to function as ultrathin membranes that can be either permeable or impermeable.[3−7] As an example of the application of impermeable membranes, monolayer graphene has been used as a conformal coating to encapsulate and protect nanowires,[8] perovskites,[9] other 2D layers,[10] and single organic microcrystals.[11] This conductive coating enabled the crystals to be visualized directly using electron microscopy, protected them from solvent attack, and prevented sublimation at elevated temperatures. In principle, the single atom thick coating would enable routine characterization of exciton dynamics in the crystal using near-field optical and scanning probe microscopy techniques under ambient conditions. Graphene encapsulation, however, has one major drawback: as a semi-metal, graphene is expected to perturb the electronic states and photophysical behavior of the underlying crystal, at least near the surface.

If our goal is to study the intrinsic exciton dynamics of an organic crystal, an electronically inert coating must be used. Hexagonal boron nitride (h-BN) is a 2D material whose large band gap (>5 eV)[12] should allow easy optical access while avoiding energy and electron-transfer processes that can quench electronic excited states. It has been used successfully to encapsulate and protect other 2D materials,[13−15] metal surfaces,[16] and layered perovskites.[17] However, h-BN's weaker mechanical properties and higher propensity to fracture[18,19] make it more challenging to use it to encapsulate a three-dimensional object such as a molecular crystal. We were not sure whether h-BN's susceptibility to structural defects and fracture during the encapsulation process would prevent its use for protective encapsulation of single crystals.

In this work, we examine the ability of different h-BN samples to cover single perylene (PER) microcrystals. We characterize the sample morphology and chemical stability using electron, optical, and atomic force microscopies. To determine the interaction of the 2D material with the underlying organic chromophores, a polymer film assay is used to characterize the fluorescence quenching ability of both graphene and h-BN. The

Received: July 11, 2020
Revised: August 18, 2020
Published: August 21, 2020

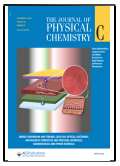

https://dx.doi.org/10.1021/acs.jpcc.0c06346
J. Phys. Chem. C 2020, 124, 21170−21177

most surprising result is that solution-transferred h-BN is not photophysically inert but instead has an effective Forster quenching radius of 2.9 nm, as compared to 14.6 nm for graphene. However, the fluorescence quenching can be completely avoided by using dry-transfer methods. Both the source of h-BN and its method of transfer determine its ability to act as an inert coating and avoid fluorescence quenching. Encapsulation of organic solids using multilayer h-BN is feasible, but attention must be paid to preparation conditions and the nature of the h-BN sample.

EXPERIMENTAL SECTION

Sample Preparation. To prepare isolated perylene microcrystals, a PER/acetone solution (10^{-3} M) was drop-cast onto a glass substrate, which was dried in air. Chemical vapor deposition (CVD) grown monolayer graphene, monolayer h-BN, and multilayer h-BN were purchased from Graphene Supermarket. Additional multilayer h-BN samples were grown on a Ni substrate using the molecular beam epitaxy (MBE) method, as described previously.[20,21] To make polymer−dye films for the fluorescence quenching studies, the dye Lumogen Red (LR) (BASF Lumogen F Red 305) and the polymer poly(methyl methacrylate) (PMMA; MW ≈ 120000 g/mol; Sigma-Aldrich) were co-dissolved in toluene at an appropriate weight percentage of LR:PMMA ≈ 1:1200. The solution was then diluted with toluene into lower concentrations. The resulting solutions had different viscosities and were spin-coated onto the glass substrate at 500−4000 rpm to make solid films with different thicknesses but with the same dye concentration ≈ 1 mM. The final thickness of the polymer layer was measured using atomic force microscopy.

2D Material Transfer. Two different methods, wet and dry, were used to place the 2D materials in contact with the organic component. In the wet-transfer method, a thin (∼200 nm) layer of PMMA (Microchem 950 PMMA A4) was spin-coated onto commercially available graphene and h-BN grown by chemical vapor deposition on a Cu substrate or onto MBE-grown h-BN on a Ni substrate. The metal support was then chemically etched away using an aqueous solution of HCl (5 wt % in water) and $FeCl_3$ (0.3 M). The etching solution was replaced by deionized water to rinse the 2D samples, and this replacement could be repeated multiple times to extract any remaining metal ions. The previously prepared glass substrate with PER crystals was then used to lift up the floating 2D layer. The substrate with its transferred 2D layer was dried in air for 30 min and then immersed in acetone for 1 h to dissolve the PMMA layer. Finally, the substrate was dried with a gentle air flow. For the dry transfer of h-BN, the h-BN layer on Ni was first exfoliated using silicone-free adhesive film (Ultron Systems Inc.). Then the adhesive film was firmly pressed onto the SiO_2/Si substrate using cotton swabs. The adhesive film was peeled away slowly and the h-BN flakes that remained on the SiO_2/Si substrate were coated with the fluorescent polymer layer.

Sample Characterization. Optical and fluorescence microscopy images were taken using an Olympus BX51W1 microscope. Fluorescence images were taken using either a fluorescein isothiocyanate (FITC) filter cube (resulting in a green image) or a rhodamine conjugate U-MNG filter cube (resulting in a red image). Scanning electron microscopy (SEM) image collection was performed using a Leo XB 1540 focused ion beam milling system with 3 kV electron beam voltage. Atomic force microscopy (AFM) images were collected in tapping mode using a Digital Instruments Nanoscope IIIA scanned probe microscope system (AFM probe: NSG01, NT-MDT Spectrum Instruments). Cross-sectional analysis was performed using the Nanoscope Control software.

Spectroscopic characterization of the samples was performed using several different instruments. Steady-state fluorescence spectra were collected using a Nicolet Almega XR dispersive Raman microscope with 532 nm laser excitation through a 50× objective (numerical aperture (NA) = 0.8) with an estimated focus size of 1 μm. Time-resolved fluorescence experiments were conducted using the time-correlated single photon counting technique. The output of a laser oscillator (Light Conversion Inc., Pharos) at a central wavelength of 1030 nm, with 76 MHz repetition rate and ∼90 fs pulse duration, was frequency-doubled to 515 nm. These pulses were directed through an integrated microscope system with a 40× objective (NA = 0.6) and used to excite localized sample areas on the order of 1 μm in diameter. The fluorescence signal was detected with an avalanche photodiode (PicoQuant, PDM) and its temporal trace measured by a time-correlated single photon counting module (PicoQuant, PicoHarp 300).

X-ray photoelectron spectroscopy (XPS) characterization was carried out using a Kratos AXIS ULTRADLD XPS system equipped with an Al Kα monochromatic X-ray source and a 165 mm mean radius electron energy hemispherical analyzer. The vacuum pressure was kept below 3×10^{-9} Torr during the acquisition. A neutralizer was also applied to compensate for charging during the measurement.

RESULTS AND DISCUSSION

Plate-like PER microcrystals in the α crystal polymorph form,[22] grown by solvent evaporation on a glass substrate, have been previously shown to be amenable to graphene encapsulation. The crystals were encapsulated under h-BN using the same wet-transfer process developed in our previous work.[11] When this method was used for CVD-grown graphene, a high yield of encapsulated PER microcrystals was obtained. But when used for the CVD-grown monolayer and bilayer h-BN, no PER crystals survived after exposure to acetone. Optical microscopy revealed that h-BN layers were present on the glass slide, but they could not prevent dissolution of the organic crystals, suggesting that they had a high density of holes that allowed the solvent to penetrate.

In order to determine whether different forms of h-BN could be used in the wet-transfer encapsulation process, we turned to multilayer h-BN grown by MBE onto a metal foil. These samples have been shown to cover large areas with mechanically intact h-BN up to 10 layers thick (Supporting Information Figure S1).[23] Using this MBE-grown h-BN and the same wet-transfer method, we could demonstrate successful encapsulation. Figure 1 summarizes the results of this series of experiments. The square PER crystals can be directly imaged using SEM without a conductive coating. Similar to graphene, the high carrier mobility in h-BN prevents surface charge build up in the low-conductivity organic at low electron beam voltages (<5 kV).[11] Also similar to graphene, AFM images reveal that the h-BN adheres as a conformal coating, with the sharp edges of the underlying crystal clearly visible. The ability of h-BN to conformally encapsulate the PER crystals was somewhat surprising in light of the fact that the MBE-grown h-BN has multiple layers, which would tend to reduce its flexibility.[18]

Successful encapsulation was confirmed by the fact that the encapsulated PER crystals were unaffected by solvent exposure or elevated temperatures. Figure 2 shows fluorescence

https://dx.doi.org/10.1021/acs.jpcc.0c06346
J. Phys. Chem. C 2020, 124, 21170−21177

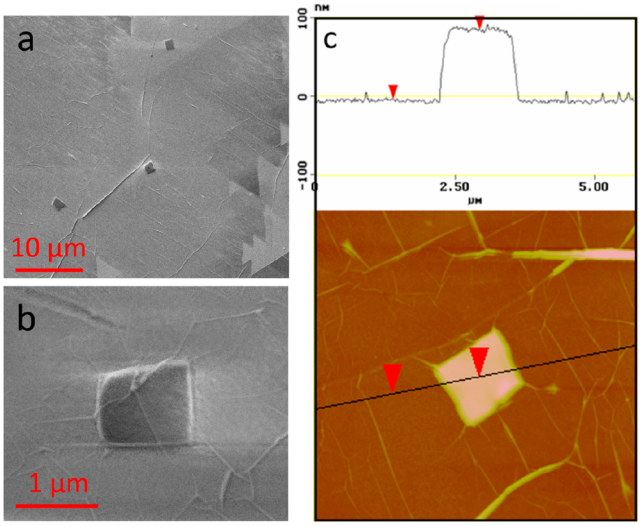

Figure 1. Characterization of MBE-grown h-BN encapsulated PER crystals. (a) SEM image of multiple PER crystals (dark spots) under h-BN; (b) SEM image of single PER crystal showing wrinkles in h-BN layer; (c) AFM scanning image and cross-section of a single encapsulated PER crystal, also showing the wrinkles of the h-BN layer that extend onto the top of the crystal. The typical crystal size is around 2 μm^2 with 100 nm height.

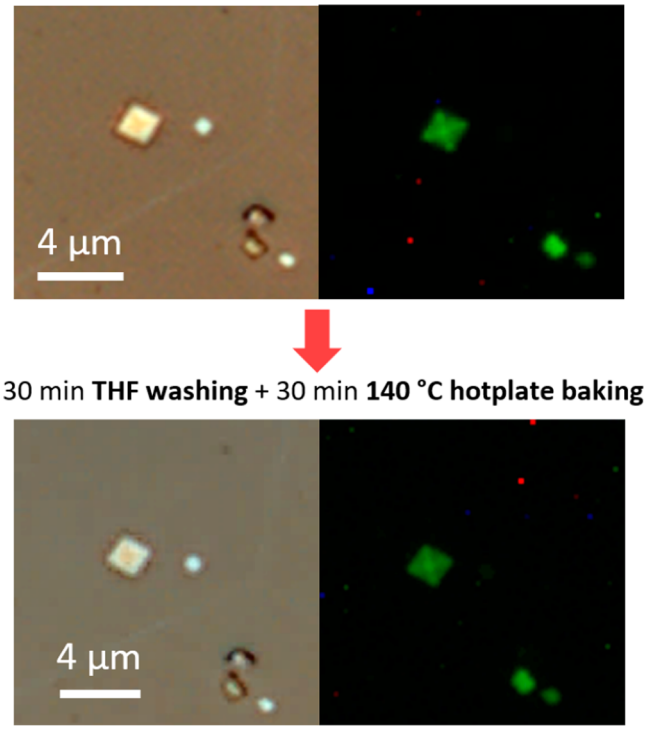

Figure 2. Reflectance and fluorescence microscopy images showing how encapsulation by MBE-grown h-BN enhances the stability of PER microcrystals. Encapsulated crystals can survive 30 min THF bath washing plus 30 min hot plate baking at 140 °C without significant loss of fluorescence intensity.

microscopy images of PER microcrystals that have been encapsulated under MBE-grown h-BN. Neither immersion in tetrahydrofuran for 30 min nor heating to 140 °C in air had a noticeable effect on the PER fluorescence intensity. Without encapsulation, the microcrystals vanished within 5 min under the same conditions. These measurements confirm that MBE-grown h-BN can function as a protective covering for the organic crystals, similar to monolayer graphene. The main difference is that the yield of encapsulated crystals is about 95% lower than that for CVD-grown monolayer graphene, possibly due to a larger number of holes resulting from defects and/or fracture during the transfer process.

After demonstrating that h-BN encapsulation can provide chemical protection, we next had to determine whether it was electronically inert, since the goal was to have an ultrathin coating that did not interact with the organic crystal through energy or charge transfer. One way to assess the presence of such interactions is to look for fluorescence quenching by the 2D layer. Previously, we found that the overall fluorescence decays of single PER crystals were unaffected by the presence of a graphene overlayer.[11] Those measurements probed relatively thick (>100 nm) crystals, however, and could not rule out quenching of a surface layer of up to 20 nm by the graphene. Given the difficulty of growing PER crystals with thicknesses < 20 nm,[24] where fluorescence quenching would become apparent, we turned to a different strategy to assess how the 2D layers interact with molecular excited states.

Figure 3 outlines our experimental approach to measure surface quenching by a 2D layer. Instead of using a molecular

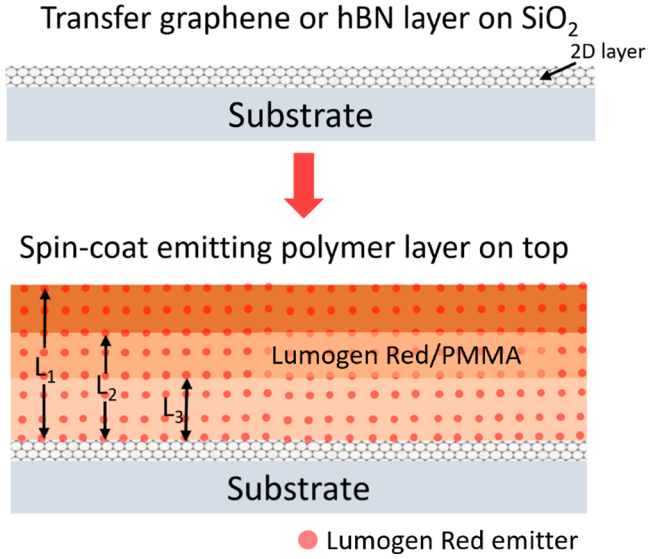

Figure 3. Schematic of the 2D layer/emitting polymer sample used to extract the fluorescence quenching radius of graphene and h-BN. Lumogen Red/PMMA emitting layers with different thicknesses (L) were spin-coated onto the 2D layers, and the average fluorescence lifetime depends on L and the quenching radius (R_0).

crystal, we used a spin-cast polymer film consisting of PMMA doped with the dye molecule Lumogen Red (LR). The thickness of the polymer film can be controlled by the concentration of the precursor solution and the spin-coating conditions.[25] The concentration of the dye was kept low enough (<1 mM[26]) to prevent intermolecular energy migration within the film. Under these conditions, each dopant was quenched individually by the 2D material on the surface without the complicating factor of energy migration that might amplify the quenching effect. The time-dependent excited-state population of a molecule at distance R from the quenching layer, $N_{ex}(R,t)$ subject to a distance-dependent quenching rate $k_q(R)$, is given by[27]

$$N_{ex}(R, t) = N_0 \exp[-k_{fl}t - k_q(R)t] \quad (1)$$

https://dx.doi.org/10.1021/acs.jpcc.0c06346
J. Phys. Chem. C 2020, 124, 21170−21177

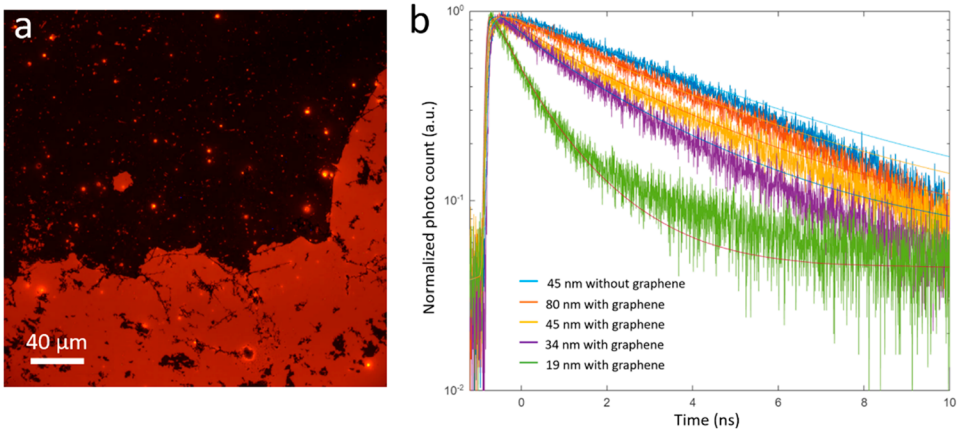

Figure 4. (a) Fluorescence microscope image of Lumogen Red (LR)/PMMA layer (L = 34 nm) on top of single layer graphene. The LR/PMMA composite is evenly spin-coated onto the substrate, but only the top half contains graphene. The area on top of graphene shows significant fluorescence quenching as compared to bare glass (bright orange). (b) Logarithmic plots of thickness-dependent fluorescence decays of LR/PMMA layer on graphene. The decay becomes faster with decreasing emitting layer thickness. Fits using eq 3 with R_0 = 14.6 nm are overlaid with the data.

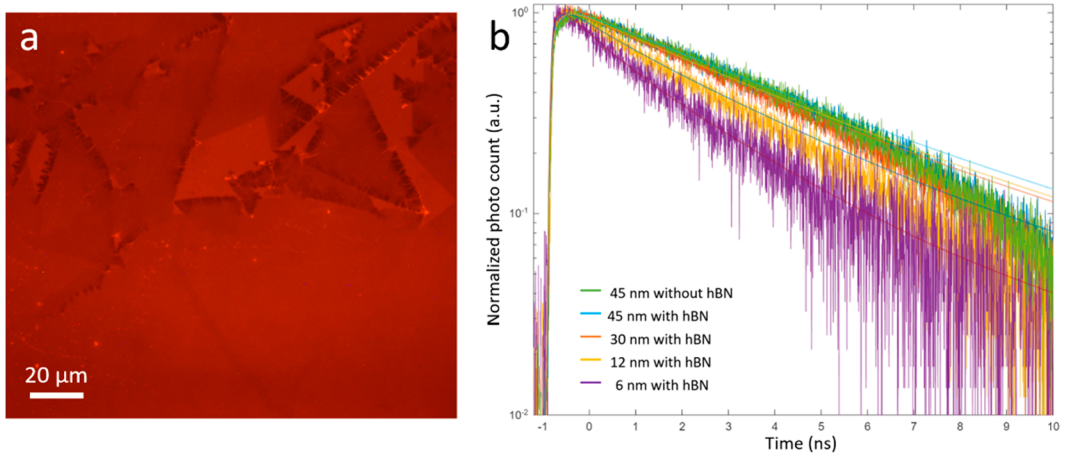

Figure 5. (a) Fluorescence microscope image of LR/PMMA layer (L = 12 nm) on top of an MBE h-BN layer. The area covered with h-BN (visible as triangular outlines) shows slight fluorescence quenching; (b) logarithmic plots of thickness-dependent fluorescence decays of LR/PMMA layer on MBE-grown h-BN using the wet-transfer method. The decay becomes faster with decreasing emitting layer thickness. Fits using equation 3 with R_0 = 2.9 nm are overlaid with the data.

k_{fl} is the intrinsic molecular fluorescence decay rate in the absence of quenching, and $k_q(R)$ is assumed to result from Forster electronic energy transfer from a dipole to a 2D surface and is given by the equation[28,29]

$$k_q(R) = \left(\frac{R_0}{R}\right)^4 \tag{2}$$

To calculate the fluorescence signal $S(t)$ for the dye/polymer film, we sum over all possible distances R from the top quenching layer,

$$S(t) = \sum_{R=0}^{L} N_{ex}(R, t) \tag{3}$$

For this summation, R was stepped in 0.1 nm increments from 0 to the film thickness L. R_0 was the only parameter that was varied to simulate the $S(t)$ curves for different values of L. In this way we could extract a self-consistent value for the quenching radius R_0 from the experimental fluorescence decays.

Figure 4a shows a fluorescence microscope image of an LR/PMMA film spin-coated on top of a graphene layer that had been placed on a glass surface using the wet-transfer method, i.e., lift-off from an aqueous solution. The regions with no graphene coverage appeared red due to the characteristic LR emission, while the regions with graphene appeared dark, suggesting strong fluorescence quenching. The time-resolved fluorescence decays shown in Figure 4b confirm that the graphene layer leads to detectable fluorescence quenching even in 80 nm thick polymer films, consistent with previous work.[30] For a 19 nm thick film, the fluorescence was almost completely absent. Also shown in Figure 4b are decay curves calculated using eqs 1−3 with R_0 = 14.6 ± 1.0 nm. As expected, the decays are not single exponential. The calculated curves do a good job of reproducing the experimental trends but clearly overestimate the fluorescence signal at longer time delays. The value of the quenching radius R_0 is large relative to typical molecular Forster radii but in line with values reported for energy donors such as quantum dots, where effective R_0 values range from 5 to 20 nm.[31−35] It is likely that the detailed spectroscopic properties of the energy donor (LR in our case) play a role in determining the overall quenching radius, just as they do in other Forster energy-transfer

https://dx.doi.org/10.1021/acs.jpcc.0c06346
J. Phys. Chem. C 2020, 124, 21170−21177

systems, but we did not attempt to model the fluorescence quenching in terms of molecular properties.

The fact that the polymer−dye method gave reasonable values for graphene was encouraging. We then spin-coated an LR/PMMA film on top of an MBE-grown h-BN layer that had been placed on a glass surface using the wet-transfer method. In Figure 5a, a fluorescence microscope image of the LR/PMMA film shows that the presence of the h-BN diminished but did not extinguish the red fluorescence. Time-resolved measurements confirmed that the effect of the h-BN on the LR/PMMA fluorescence lifetime was much less pronounced than with graphene. Figure 5b shows the fluorescence decays of various thickness LR/PMMA films on top of MBE-grown h-BN. As with graphene, there was a systematic decrease in lifetime as the polymer thickness decreased and more LR molecules found themselves close to the surface. Also shown are the decay curves calculated for R_0 = 2.9 nm, which do a good job of reproducing the observed trend with thickness.

Although the fluorescence decays are not single exponentials, for the sake of comparison we extracted an effective lifetime by fitting the first natural log of the decay to a straight line, as shown in Supporting Information Figure S8. The slope of this initial exponential region of the decay gave the effective lifetime that we plot as a function of polymer layer thickness in Figure 6. The strong dependence of the effective lifetime on thickness reflects averaging the R^4 distance dependence across the different thicknesses. Finally, we note that absolute fluorescence intensity comparisons between different samples are challenging because the detected signal is very sensitive to the details of focusing and the presence of scattering defects in the field of view. Nevertheless, the trend in fluorescence lifetime is mirrored by the trend in fluorescence signal intensity, as shown in Supporting Information Figures S9 and S10.

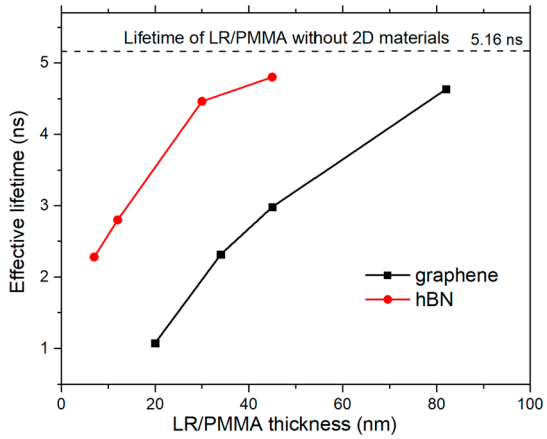

Figure 6. Thickness dependence of the effective fluorescence lifetime of the LR/PMMA layer on top of graphene and h-BN. The dashed line represents the intrinsic lifetime of the LR/PMMA layer in the absence of a 2D material.

The R_0 for the h-BN layers was about 5× smaller than that of graphene, but it was surprising to see any quenching at all. h-BN's large band gap of 5.9 eV should prevent direct energy transfer. Its low-lying valence band and high conduction band should likewise preclude electron transfer to or from the excited LR molecule (Supporting Information Figure S3).[36,37] Furthermore, any fluorescence quenching based on electron transfer would be expected to be very short range, typically <1 nm. The relatively large distances observed here are consistent with through-space energy transfer as assumed in our model. For graphene, this is expected since it is a semi-metal that has a high density of states that can accept energy from a wide variety of luminescent donors. For pristine h-BN, however, there should be no acceptor states in the 2.0 eV energy range.

Here we consider two possible origins of the energy accepting states that quench the LR fluorescence. The first possibility is that chemical impurities left over from the transfer process act as energy acceptors. The wet-transfer method used here has the advantage of being able to transfer large areas of 2D materials quickly and reproducibly.[38] But the solvent and ions may become trapped between the 2D layer and the crystal. However, we could not find any evidence that extrinsic chemical species, for example Ni ions, were responsible for the fluorescence quenching. X-ray photoelectron spectroscopy measurements on coated substrates failed to reveal any detectable signature of Ni or any other elements besides B and N (Supporting Information Figures S4 and S5). After dissolution of the Ni substrate, h-BN was subjected to repeated solvent replacements to remove any residual species leftover from the etching process, but the amount of fluorescence quenching was insensitive to the number of times the transfer solvent was exchanged in the h-BN rinsing step.

A second possibility is that defects in the h-BN itself are responsible for the quenching. Recent studies have shown that most h-BN samples contain defects that luminesce in the visible

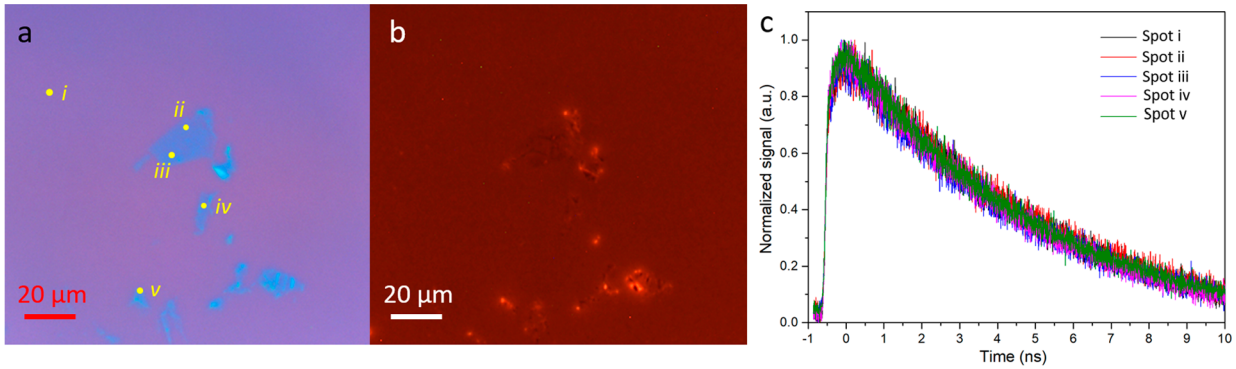

Figure 7. (a, b) Reflectance and fluorescence microscopy images of an LR/PMMA layer (L = 10 nm) on exfoliated MBE-grown h-BN placed on glass using the dry-transfer method. (c) Fluorescence decays of the LR/PMMA layer at different locations: spot i, location where only the polymer layer is located; spots ii−v, locations where the h-BN lies underneath the polymer. The brighter spots in panels a and b are from aggregation of polymer on the edge and wrinkles of the h-BN flakes and are avoided during the fluorescence measurement.

https://dx.doi.org/10.1021/acs.jpcc.0c06346
J. Phys. Chem. C 2020, 124, 21170−21177

wavelength range with nanosecond lifetimes and high quantum yields.[39−41] It is not unreasonable to expect that the strong radiative rate of the defect is accompanied by a strong absorption as well. Various defects, whose exact structure is a topic of active investigation, could also act as energy acceptors for the excited LR molecules. Note that all that is required is a concentration of absorbing defect states—they do not have to be emissive and in fact may be completely different from the luminescent defects that are more commonly studied. These defects may be present as vacancies and grain boundaries when the h-BN is grown, as proved by trap-assisted tunneling current studies,[42] or they may be introduced during the sample processing. For example, the floating, lift-off, and subsequent solvent dissolution of the polymer layer can all induce transient stress in the 2D layer and create defects along the way.

If the LR fluorescence is being quenched by defect states in the h-BN, then changing the method of preparation to reduce defect density should reduce the fluorescence quenching as well. Dry-transfer methods provide the gentlest way to transfer 2D materials,[43,44] but they are more labor intensive, producing smaller flakes that must be individually positioned and deposited. The h-BN flakes produced in this way are usually too small for complete crystal encapsulation, but it was possible to examine whether they quenched the fluorescence. The fluorescence lifetime was measured at various locations in LR/PMMA films that had been spin-coated on top of several h-BN flakes. None of the decays in Figure 7c show measurable quenching of the LR fluorescence, whether on top of the h-BN or not. This result suggests that the defects that lead to fluorescence quenching are indeed introduced via the wet-transfer method and can be avoided by using dry transfer. Unfortunately, the relatively small h-BN flakes and our current imprecise method of positioning them made it impossible to use them for PER crystal encapsulation. Recently developed methods for the growth and transfer of large h-BN flakes with diameters on the order of 100 μm[45,46] may make it possible to completely cover a single crystal and seal it from the surrounding substrate.

CONCLUSION

The results reported here show that, like graphene, ultrathin layers of h-BN can be used to fully encapsulate single organic crystals. Successful encapsulation depends on the quality of the h-BN, and we found that only multilayer MBE-grown h-BN could fully protect the crystals from dissolution and sublimation. Investigation of the effects of these 2D coatings on the fluorescence signal of thin dye/polymer films revealed that the wet-transfer method likely produces structural defects in the h-BN that act as fluorescence quenching sites. This quenching could be avoided by the use of a dry-transfer method, which we hope will enable the encapsulation of single crystals under a truly inert, transparent coating. The results of this work represent a step forward in our efforts to integrate 2D materials with molecular crystals in order to create new platforms for the measurement of their electronic properties.

ASSOCIATED CONTENT

Supporting Information

The Supporting Information is available free of charge at https://pubs.acs.org/doi/10.1021/acs.jpcc.0c06346.

AFM characterizations of h-BN thickness and Lumogen Red/PMMA thicknesses; energy level diagram of h-BN and perylene; XPS characterizations of wet-transferred MBE h-BN; Instrument response function convolution example; SEM of h-BN; fitting for effective lifetimes; fluorescence intensity comparison of Lumogen Red/PMMA with different 2D materials and thicknesses (PDF)

AUTHOR INFORMATION

Corresponding Author

Christopher J. Bardeen − *Department of Chemistry, University of California Riverside, Riverside, California 92521, United States;* orcid.org/0000-0002-5755-9476; Email: christopher.bardeen@ucr.edu

Authors

Wangxiang Li − *Department of Chemistry, University of California Riverside, Riverside, California 92521, United States;* orcid.org/0000-0002-6601-6860

Hao Tian − *Department of Electrical and Computer Engineering, University of California Riverside, Riverside, California 92521, United States;* orcid.org/0000-0001-5893-2319

Jeremiah van Baren − *Department of Physics and Astronomy, University of California Riverside, Riverside, California 92521, United States*

Adam Berges − *Department of Chemistry, University of California Riverside, Riverside, California 92521, United States*

Mashael M. Altaiary − *Department of Physics and Astronomy, University of California Riverside, Riverside, California 92521, United States*

Erfu Liu − *Department of Physics and Astronomy, University of California Riverside, Riverside, California 92521, United States;* orcid.org/0000-0002-0231-798X

Elena Bekyarova − *Department of Chemistry, University of California Riverside, Riverside, California 92521, United States;* orcid.org/0000-0001-7565-2773

Chun Hung Lui − *Department of Physics and Astronomy, University of California Riverside, Riverside, California 92521, United States*

Jianlin Liu − *Department of Electrical and Computer Engineering, University of California Riverside, Riverside, California 92521, United States;* orcid.org/0000-0001-6513-0867

Complete contact information is available at: https://pubs.acs.org/10.1021/acs.jpcc.0c06346

Notes

The authors declare no competing financial interest.

ACKNOWLEDGMENTS

This work was supported by the National Science Foundation Grants CHE-1800187 (C.J.B.) and DMR-1945660 (CAREER) (C.H.L.).

REFERENCES

(1) Butler, S. Z.; Hollen, S. M.; Cao, L.; Cui, Y.; Gupta, J. A.; Gutierrez, H. R.; Heinz, T. F.; Hong, S. S.; Huang, J.; Ismach, A. F.; et al. Progress, Challenges, and Opportunities in Two-Dimensional Materials Beyond Graphene. *ACS Nano* **2013**, *7*, 2898−2926.

(2) Zhuang, X.; Mai, Y.; Wu, D.; Zhang, F.; Feng, X. Two-Dimensional Soft Nanomaterials: A Fascinating World of Materials. *Adv. Mater.* **2015**, *27*, 403−427.

(3) Berry, V. Impermeability of Graphene and its Applications. *Carbon* **2013**, *62*, 1−10.

(4) Bunch, J. S.; Verbridge, S. S.; Alden, J. S.; van der Zande, A. M.; Parpia, J. M.; Craighead, H. G.; McEuen, P. L. Impermeable Atomic Membranes from Graphene Sheets. *Nano Lett.* **2008**, *8*, 2458−2462.
(5) Dervin, S.; Dionysiou, D. D.; Pillai, S. C. 2D Nanostructures for Water Purification: Graphene and Beyond. *Nanoscale* **2016**, *8*, 15115−15131.
(6) Prozorovska, L.; Kidambi, P. R. State-of-the-Art and Future Prospects for Atomically Thin Membranes from 2D Materials. *Adv. Mater.* **2018**, *30*, 1801179.
(7) Wang, S.; Yang, L.; He, G.; Shi, B.; Li, Y.; Wu, H.; Zhang, R.; Nunes, S.; Jiang, Z. Two-Dimensional Nanochannel Membranes for Molecular and Ionic Separations. *Chem. Soc. Rev.* **2020**, *49*, 1071−1089.
(8) Deng, B.; Hsu, P.-C.; Chen, G.; Chandrashekar, B. N.; Liao, L.; Ayitimuda, Z.; Wu, J.; Guo, Y.; Lin, L.; Zhou, Y.; et al. Roll-to-Roll Encapsulation of Metal Nanowires between Graphene and Plastic Substrate for High-Performance Flexible Transparent Electrodes. *Nano Lett.* **2015**, *15*, 4206−4213.
(9) Shen, X.; Wang, M.; Zhou, F.; Qiu, B.; Cai, L.; Liu, Y.; Zheng, Z.; Chai, Y. Improved Air-Stability of an Organic-Inorganic Perovskite with Anhydrously Transferred Graphene. *J. Mater. Chem. C* **2018**, *6*, 8663−8669.
(10) Xia, K.; Jian, M.; Wang, C.; Yin, Z.; Zhang, M.; Wang, H.; Wu, Y.; Zhang, Y. Seamless Graphene-Seal-Wrap as a Removable Protective Cover for Two-Dimensional Materials. *ACS Materials Lett.* **2020**, *2*, 215−219.
(11) Li, W.; Tierce, N. T.; Bekyarova, E.; Bardeen, C. J. Protection of Molecular Microcrystals by Encapsulation under Single-Layer Graphene. *ACS Omega* **2018**, *3*, 8129−8134.
(12) Cassabois, G.; Valvin, P.; Gil, B. Hexagonal Boron Nitride is an Indirect Bandgap Semiconductor. *Nat. Photonics* **2016**, *10*, 262−266.
(13) Petrone, N.; Chari, T.; Meric, I.; Wang, L.; Shepard, K. L.; Hone, J. Flexible Graphene Field-Effect Transistors Encapsulated in Hexagonal Boron Nitride. *ACS Nano* **2015**, *9*, 8953−8959.
(14) Lee, G. H.; Cui, X.; Kim, Y. D.; Arefe, G.; Zhang, X.; Lee, C.-H.; Ye, F.; Watanabe, K.; Taniguchi, T.; Kim, P.; et al. Highly Stable, Dual-Gated MoS_2 Transistors Encapsulated by Hexagonal Boron Nitride with Gate-Controllable Contact, Resistance, and Threshold Voltage. *ACS Nano* **2015**, *9*, 7019−7026.
(15) Chen, X.; Wu, Y.; Wu, Z.; Han, Y.; Xu, S.; Wang, L.; Ye, W.; Han, T.; He, Y.; Cai, Y.; et al. High-Quality Sandwiched Black Phosphorus Heterostructure and its Quantum Oscillations. *Nat. Commun.* **2015**, *6*, 7315.
(16) Liu, Z.; Gong, Y.; Zhou, W.; Ma, L.; Yu, J.; Idrobo, J. C.; Jung, J.; MacDonald, A. H.; Vajtai, R.; Lou, J.; et al. Ultrathin High-Temperature Oxidation-Resistant Coatings of Hexagonal Boron Nitride. *Nat. Commun.* **2013**, *4*, 2541.
(17) Fang, H.-H.; Yang, J.; Tao, S.; Adjokatse, S.; Kamminga, M. E.; Ye, J.; Blake, G. R.; Even, J.; Loi, M. A. Unravelling Light-Induced Degradation of Layered Perovskite Crystals and Design of Efficient Encapsulation for Improved Photostability. *Adv. Funct. Mater.* **2018**, *28*, 1800305.
(18) Falin, A.; Cai, Q.; Santos, E. J. G.; Scullion, D.; Qian, D.; Zhang, R.; Yang, Z.; Huang, S.; Watanabe, K.; Taniguchi, T.; et al. Mechanical Properties of Atomically Thin Boron Nitride and the Role of Interlayer Interactions. *Nat. Commun.* **2017**, *8*, 15815.
(19) Mallick, G.; Elder, R. M. Graphene/Hexagonal Boron Nitride Heterostructures: Mechanical Properties and Fracture Behavior from Nanoindentation Simulations. *Appl. Phys. Lett.* **2018**, *113*, 121902.
(20) Tian, H.; Khanaki, A.; Das, P.; Zheng, R.; Cui, Z.; He, Y.; Shi, W.; Xu, Z.; Lake, R.; Liu, J. Role of Carbon Interstitials in Transition Metal Substrates on Controllable Synthesis of High-Quality Large-Area Two-Dimensional Hexagonal Boron Nitride Layers. *Nano Lett.* **2018**, *18*, 3352−3361.
(21) Tian, H.; He, Y.; Das, P.; Cui, Z.; Shi, W.; Khanaki, A.; Lake, R. K.; Liu, J. Growth Dynamics of Millimeter-Sized Single-Crystal Hexagonal Boron Nitride Monolayers on Secondary Recrystallized Ni (100) Substrates. *Adv. Mater. Interfaces* **2019**, *6*, 1901198.
(22) Pick, A.; Klues, M.; Rinn, A.; Harms, K.; Chatterjee, S.; Witte, G. Polymorph-Selective Preparation and Structural Characterization of Perylene Single Crystals. *Cryst. Growth Des.* **2015**, *15*, 5495−5504.
(23) Xu, Z.; Tian, H.; Khanaki, A.; Zheng, R.; Suja, M.; Liu, J. Large-Area Growth of Multi-layer Hexagonal Boron Nitride on Polished Cobalt Foils by Plasma Assisted Molecular Beam Epitaxy. *Sci. Rep.* **2017**, *7*, 43100.
(24) Lei, Y.; Liao, Q.; Fu, H.; Yao, J. Phase- and Shape-Controlled Synthesis of Single Crystalline Perylene Nanosheets and Its Optical Properties. *J. Phys. Chem. C* **2009**, *113*, 10038−10043.
(25) Walsh, C. B.; Franses, E. I. Ultrathin PMMA Films Spin-Coated from Toluene Solutions. *Thin Solid Films* **2003**, *429*, 71−76.
(26) Colby, K. A.; Burdett, J. J.; Frisbee, R. F.; Zhu, L.; Dillon, R. J.; Bardeen, C. J. Electronic Energy Migration on Different Time Scales: Concentration Dependence of the Time-Resolved Anisotropy and Fluorescence Quenching of Lumogen Red in Poly(methyl methacrylate). *J. Phys. Chem. A* **2010**, *114*, 3471−3482.
(27) Piland, G. B.; Burdett, J. J.; Hung, T.-Y.; Chen, P.-H.; Lin, C.-F.; Chiu, T.-L.; Lee, J.-H.; Bardeen, C. J. Dynamics of Molecular Excitons Near a Semiconductor Surface Studied by Fluorescence Quenching of Polycrystalline Tetracene on Silicon. *Chem. Phys. Lett.* **2014**, *601*, 33−38.
(28) Swathi, R. S.; Sebastian, K. L. Long Range Resonance Energy Transfer from a Dye Molecule to Graphene has $(\text{Distance})^{-4}$ Dependence. *J. Chem. Phys.* **2009**, *130*, 086101.
(29) Malic, E.; Appel, H.; Hofmann, O. T.; Rubio, A. Förster-Induced Energy Transfer in Functionalized Graphene. *J. Phys. Chem. C* **2014**, *118*, 9283−9289.
(30) Goncalves, H.; Bernardo, C.; Moura, C.; Ferreira, R. A. S.; Andre, P. S.; Stauber, T.; Belsley, M.; Schellenberg, P. Long Range Energy Transfer in Graphene Hybrid Structures. *J. Phys. D: Appl. Phys.* **2016**, *49*, 315102.
(31) Liu, Y.; Liu, C. Y.; Liu, Y. Investigation on Fluorescence Quenching of Dyes by Graphite Oxide and Graphene. *Appl. Surf. Sci.* **2011**, *257*, 5513−5518.
(32) Kasry, A.; Ardakani, A. A.; Tulevski, G. S.; Menges, B.; Copel, M.; Vyklicky, L. Highly Efficient Fluorescence Quenching with Graphene. *J. Phys. Chem. C* **2012**, *116*, 2858−2862.
(33) Gaudreau, L.; Tielrooij, K. J.; Prawiroatmodjo, G. E. D. K.; Osmond, J.; de Abajo, F. J. G.; Koppens, F. H. L. Universal Distance-Scaling of Nonradiative Energy Transfer to Graphene. *Nano Lett.* **2013**, *13*, 2030−2035.
(34) Federspiel, F. o.; Froehlicher, G.; Nasilowski, M.; Pedetti, S.; Mahmood, A.; Doudin, B.; Park, S.; Lee, J.-O.; Halley, D.; Dubertret, B.; et al. Distance Dependence of the Energy Transfer Rate from a Single Semiconductor Nanostructure to Graphene. *Nano Lett.* **2015**, *15*, 1252−1258.
(35) Raja, A.; Montoya-Castillo, A.; Zultak, J.; Zhang, X.-X.; Ye, Z.; Roquelet, C.; Chenet, D. A.; van der Zande, A. M.; Huang, P.; Jockusch, S.; et al. Energy Transfer from Quantum Dots to Graphene and MoS_2: The Role of Absorption and Screening in Two-Dimensional Materials. *Nano Lett.* **2016**, *16*, 2328−2333.
(36) Pookpanratana, S. J.; Goetz, K. P.; Bittle, E. G.; Haneef, H.; You, L.; Hacker, C. A.; Robey, S. W.; Jurchescu, O. D.; Ovsyannikov, R.; Giangrisostomi, E. Electronic Properties and Structure of Single Crystal Perylene. *Org. Electron.* **2018**, *61*, 157−163.
(37) Mahvash, F.; Paradis, E.; Drouin, D.; Szkopek, T.; Siaj, M. Space-Charge Limited Transport in Large-Area Monolayer Hexagonal Boron Nitride. *Nano Lett.* **2015**, *15*, 2263−2268.
(38) Chen, M.; Li, G.; Li, W.; Stekovic, D.; Arkook, B.; Itkis, M. E.; Pekker, A.; Bekyarova, E.; Haddon, R. C. Large-Scale Cellulose-Assisted Transfer of Graphene Toward Industrial Applications. *Carbon* **2016**, *110*, 286−291.
(39) Jungwirth, N. R.; Fuchs, G. D. Optical Absorption and Emission Mechanisms of Single Defects in Hexagonal Boron Nitride. *Phys. Rev. Lett.* **2017**, *119*, 057401.
(40) Grosso, G.; Moon, H.; Lienhard, B.; Ali, S.; Efetov, D. K.; Furchi, M. M.; Jarillo-Herrero, P.; Ford, M. J.; Aharonovich, I.; Englund, D. Tunable and High-Purity Room Temperature Single-Photon Emission

from Atomic Defects in Hexagonal Boron Nitride. *Nat. Commun.* **2017**, *8*, 705.
(41) Exarhos, A. L.; Hopper, D. A.; Grote, R. R.; Alkauskas, A.; Bassett, L. C. Optical Signatures of Quantum Emitters in Suspended Hexagonal Boron Nitride. *ACS Nano* **2017**, *11*, 3328−3336.
(42) Cui, Z.; He, Y.; Tian, H.; Khanaki, A.; Xu, L.; Shi, W.; Liu, J. Study of Direct Tunneling and Dielectric Breakdown in Molecular Beam Epitaxial Hexagonal Boron Nitride Monolayers Using Metal-Insulator-Metal Devices. *ACS Appl. Electron. Mater.* **2020**, *2*, 747−755.
(43) Castellanos-Gomez, A.; Buscema, M.; Molenaar, R.; Singh, V.; Janssen, L.; van der Zant, H. S. J.; Steele, G. A. Deterministic Transfer of Two-Dimensional Materials by All-Dry Viscoelastic Stamping. *2D Mater.* **2014**, *1*, 011002.
(44) Kinoshita, K.; Moriya, R.; Onodera, M.; Wakafuji, Y.; Masubuchi, S.; Watanabe, K.; Taniguchi, T.; Machida, T. Dry release Transfer of Graphene and Few-Layer h-BN by Utilizing Thermoplasticity of Polypropylene Carbonate. *2D Mater. Appl.* **2019**, *3*, 22.
(45) Chen, T. A.; Chuu, C. P.; Tseng, C. C.; Wen, C. K.; Wong, H. S. P.; Pan, S.; Li, R.; Chao, T. A.; Chueh, W. C.; Zhang, Y.; et al. Wafer-Scale Single-Crystal Hexagonal Boron Nitride Monolayers on Cu (111). *Nature* **2020**, *579*, 219−223.
(46) Liu, F.; Wu, W.; Bai, Y.; Chae, S. H.; Li, Q.; Wang, J.; Hone, J.; Zhu, X. Y. Disassembling 2D Van der Waals Crystals into Macroscopic Monolayers and Reassembling into Artificial Lattices. *Science* **2020**, *367*, 903−906.

https://dx.doi.org/10.1021/acs.jpcc.0c06346
J. Phys. Chem. C 2020, 124, 21170−21177